Electronic Supplementary Information (ESI)

Unique $[Sb_6O_2S_{13}]^{12-}$ finite chain in oxychalcogenide $Ba_6Sb_6O_2S_{13}$ leading to ultra-low thermal conductivity and giant birefringence

Yong-Fang Shi,[a,b] Sheng-Hua Zhou,[a,b,c] Peng-Fei Liu,[d] Xin-Tao Wu,[a,b] Hua Lin,*[a,b] and Qi-Long Zhu*[a,b]

[a]*State Key Laboratory of Structural Chemistry, Fujian Institute of Research on the Structure of Matter, Chinese Academy of Sciences, Fuzhou 350002, China*

[b]*Fujian Science & Technology Innovation Laboratory for Optoelectronic Information of China, Fuzhou 350002, China*

[c]*University of Chinese Academy of Sciences, Beijing 100049, China*

[d]*Spallation Neutron Source Science Center, Institute of High Energy Physics, Chinese Academy of Sciences, Dongguan 523803, China*

*E-mail: linhua@fjirsm.ac.cn and qlzhu@fjirsm.ac.cn.

Electronic Supplementary Information Index

1. Experimental Section

1.1 Materials and Instruments

All reagents used in the present experiments were purchased from commercial sources and directly used without further purification. All weighing processes were completed in an anhydrous and oxygen-free glove box. The semi-quantitative energy dispersive X-ray (EDX, Oxford INCA) spectra were measured with a field emission scanning electron microscope (FESEM, JSM6700F). Powder X-ray diffraction (PXRD) analysis was carried out in a Rigaku Mini-Flex II powder diffractometer (Cu-K_α, λ = 1.5418 Å). UV-vis-NIR absorption measurement was performed in the region of 200−2500 nm at room temperature using an UV-vis-NIR spectrometer (Perkin-Elmer Lambda 950). The reflectance spectrum of the $BaSO_4$ powder was collected as the baseline and the diffuse reflectance data were converted to absorbance internally by the instrument by use of the Kubelka-Munk function.[1] The thermal stability analyses were measured on a NETZSCH STA 449C simultaneous analyser. The thermal conductivity were measured by laser flash techniques with a Netzsch LFA 457 system and calculated using the formula $\kappa = D \times C_p \times d$, where D was the measured thermal diffusivity, C_p was the heat capacity estimated using the Dulong-Petit model ($C_p = 3nR$, where n is the number of atoms per formula unit and R is the gas constant) and d was the sample density.[2] The uncertainty of the thermal conductivity k is estimated to be within 5 %, considering the uncertainties for D, C_p and d.

1.2 Synthesis of $Ba_6Sb_6O_2S_{13}$

The starting reagents BaS (99.7 %), Sb_2O_3 (99 %), and Sb_2S_3 (99 %) purchased from Aladdin China (Shanghai) Co., Ltd. were used as obtained.

After numerous explorations on the experimental conditions including starting reactant, loading ratio, annealing temperature, the optimal synthesis condition of $Ba_6Sb_6O_2S_{13}$ was established as follows: a stoichiometric mixture of 32 mmol of BaS, 11 mmol of Sb_2O_3, and 5 mmol of Sb_2S_3 in a carbonized silica crucible. The tube was then evacuated to a vacuum of 10^{-2} Pa atmosphere and sealed. Afterward, the sample was heated in a resistance furnace to 973 K over 24 h and kept at that temperature for 72 h, and subsequently cooled to 773 K at 2.5 K/h before switching off the furnace. Red-black crystals were obtained and the yield is about 95% (based on Sb). The samples were stable in air for more than 6 months, which can be verified by the analysis results of both single-crystal and powder XRD (Figure S6).

Energy-dispersive X-ray analysis of $Ba_6Sb_6O_2S_{13}$ was shown in Figure S2. The EDX results confirmed the presence of Ba, Sb, O and S in an approximate molar ratio of $Ba_{6.0(5)}Sb_{6.1(3)}O_{1.9(5)}S_{13.5(6)}$, which is in good agreement with the refined compositions obtained from the single-crystal XRD data. Compound $Ba_6Sb_6O_2S_{13}$ was characterized by powder XRD and the experimental XRD patterns of the title compound was agreed well with the simulated patterns (Figure 3b).

The as-synthesized polycrystalline samples were ground into a fine powder and hot-pressed pellet at 773 K for 60 min under an axial compressive stress of 100 MPa in vacuum. A highly dense disk (more than 95% theoretical density), with dimensions

of 10 mm in diameter and approximately 1 mm in thickness, was obtained. Graphite was evenly sprayed on both sides of the disk for the purpose of measuring thermal conductivity.

1.3 Single-Crystal Structure Characterizations

Suitable single crystal of the title compound was mounted on the glass fibers. Diffraction data were collected by an Oxford Xcalibur (Atlas Gemini ultra) diffractometer with a graphite-monochromated Mo-K_α radiation (λ = 0.71073 Å) at room temperature. The absorption correction was based on the multi-scan method.[3] The structures were solved by the direct methods and refined by the full-matrix least-squares fitting on F^2 using the *SHELXL-2014* software package.[4] The assignments of Ba, Sb, O, and S were determined on the basis of the interatomic distances, coordination environments and relative displacement parameters. The structure was verified using the *ADDSYM* algorithm from the program *PLATON*.[5] The final atomic positions were standardized with the *STRUCTURE TIDY* program.[6] Crystal data and refinement details are summarized in Tables 1-2, the selected bond lengths are listed in Table S1. CCDC number: 2247687.

2. Computational Details

Crystallographic data determined by single-crystal XRD were used for theoretical calculations of their electronic band structures. The density functional theory (DFT) calculations have been performed using the *Vienna ab initio simulation package* (VASP)[7-9] with the Perdew-Burke-Ernzerhof (PBE)[10] exchange correlation functional. The projected augmented wave (PAW)[11] potentials have been used to treat the ion-

electron interactions. A Γ-centered 7×7×9 Monkhorst-Pack grid for the Brillouin zone[12] sampling and a cutoff energy of 750 eV for the plane wave expansion were found to get convergent lattice parameters and self-consistent energies.

3. Figures and Tables

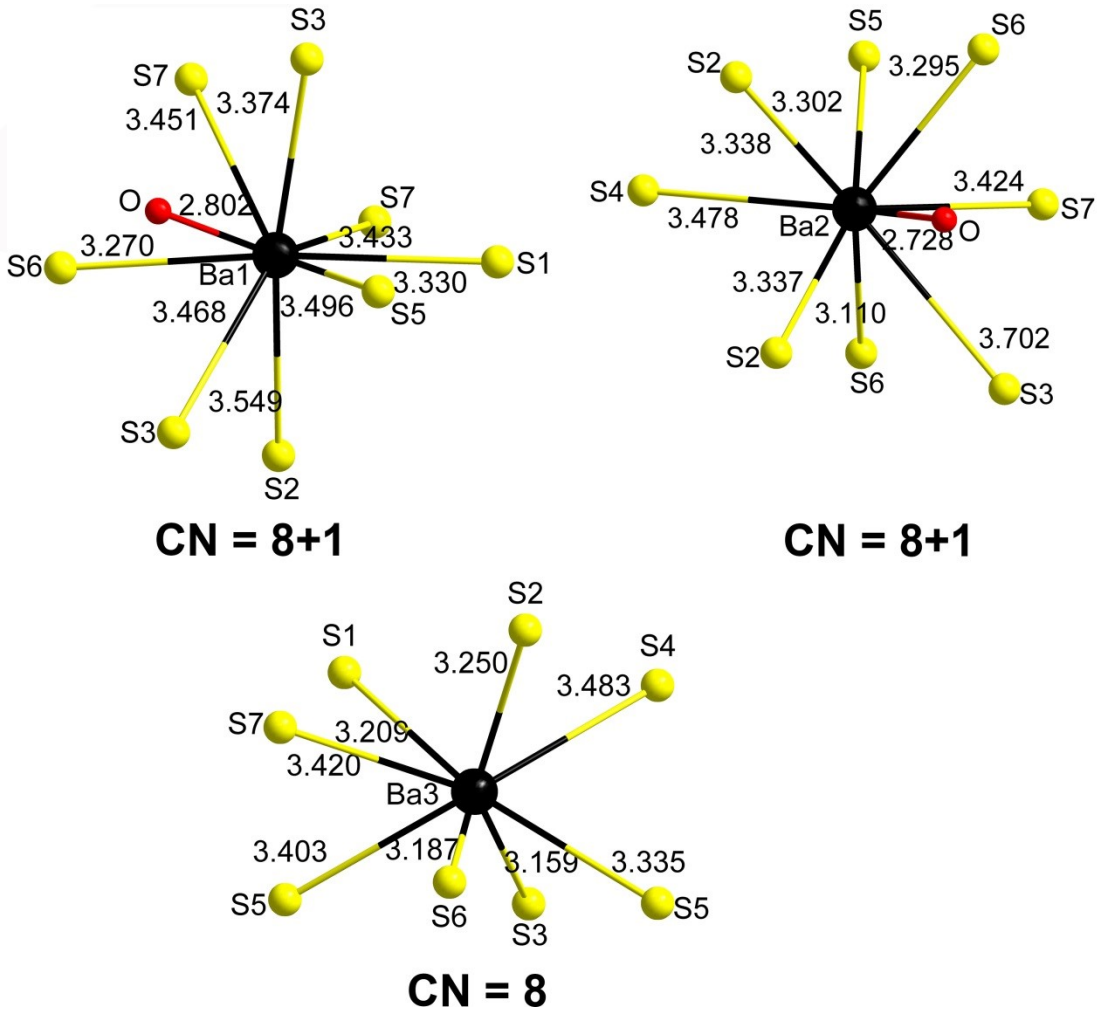

Figure S1. (a) Coordination environment of Ba atoms including bond distances in the $Ba_6Sb_6O_2S_{13}$.

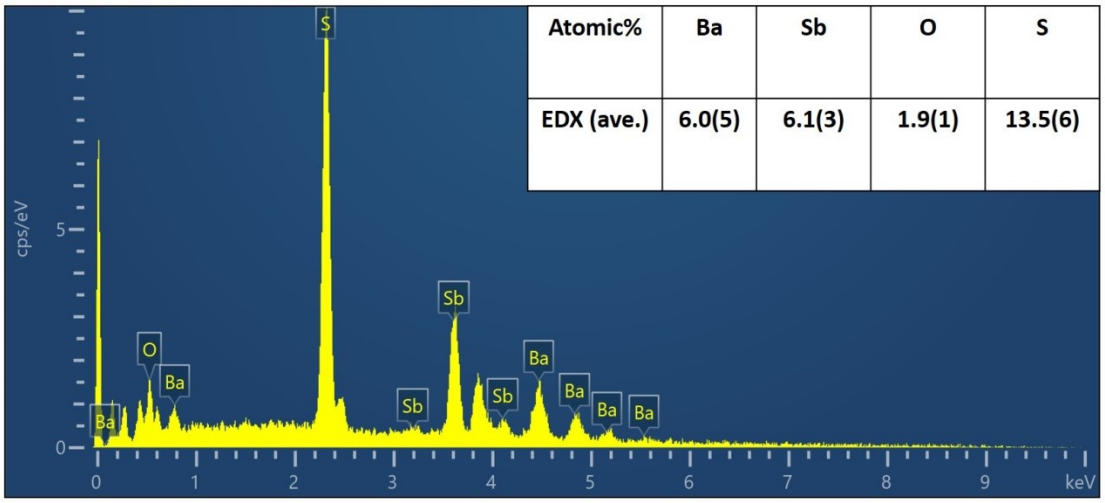

Atomic%	Ba	Sb	O	S
EDX (ave.)	6.0(5)	6.1(3)	1.9(1)	13.5(6)

Figure S2. Energy-dispersive X-ray spectroscopy analysis of $Ba_6Sb_6O_2S_{13}$.

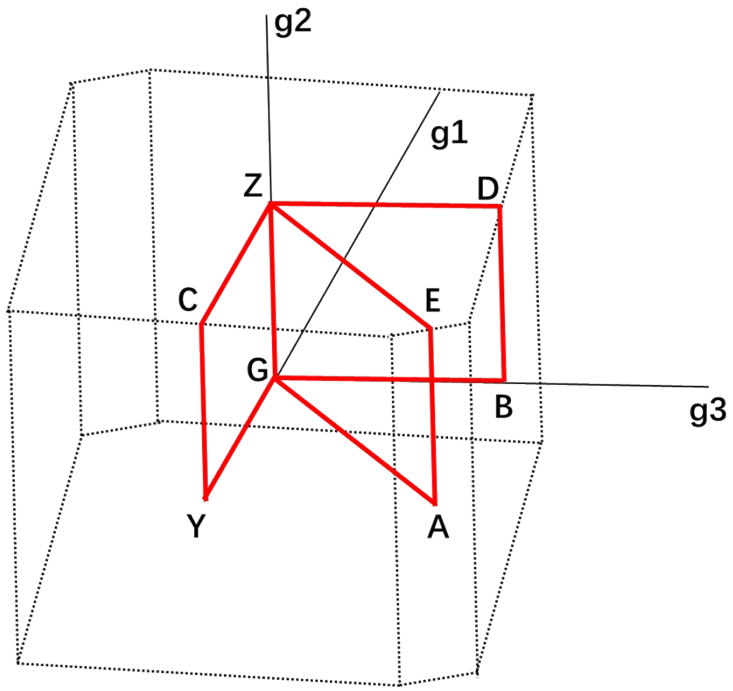

Figure S3. The first Brillouin zone with high symmetry points (red) in $Ba_6Sb_6O_2S_{13}$.

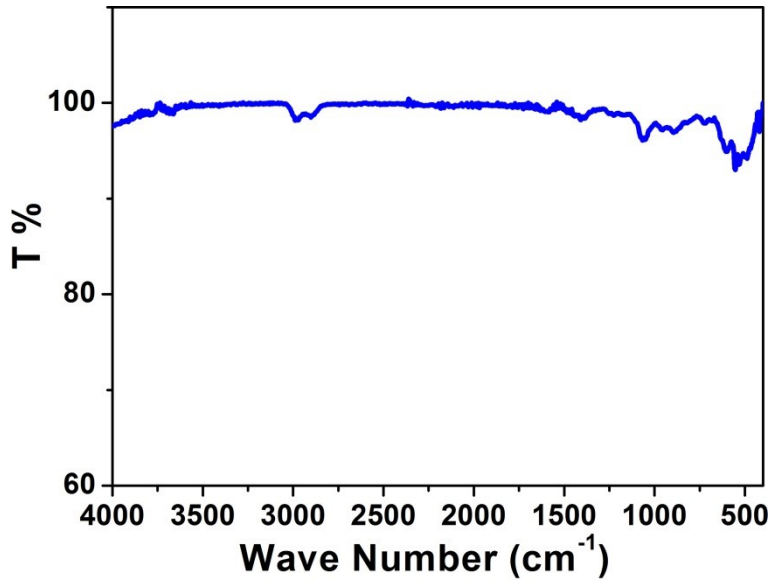

Figure S4. IR transmittance spectra of $Ba_6Sb_6O_2S_{13}$.

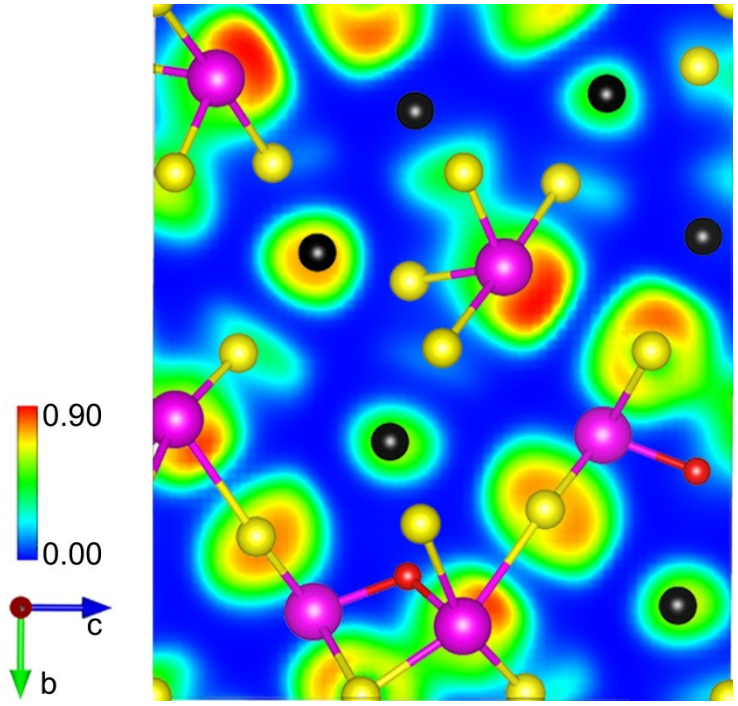

Figure S5. Electron localization function diagram of $Ba_6Sb_6O_2S_{13}$.

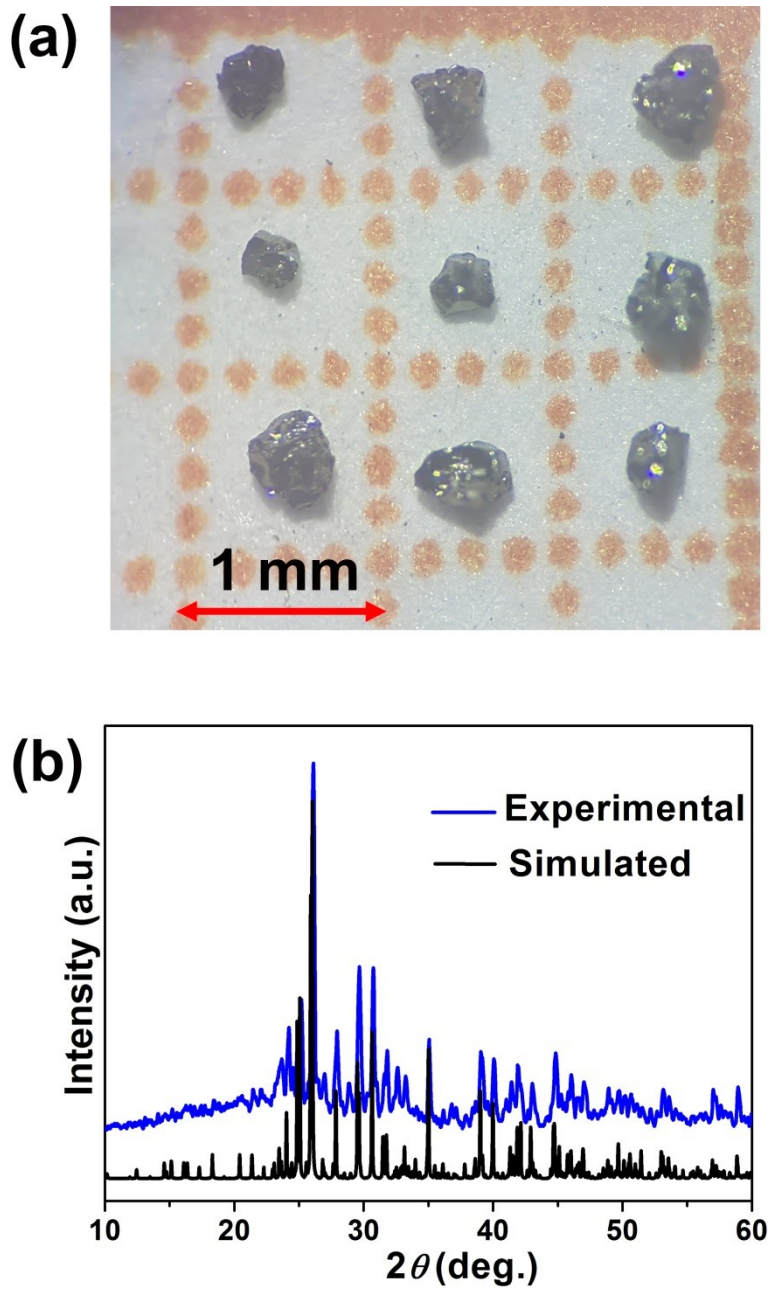

Figure S6. (a) Photograph of the title crystals and (b) powder XRD patterns of $Ba_6Sb_6O_2S_{13}$ after 6 months.

Table S1. Selected bond lengths (Å) for $Ba_6Sb_6O_2S_{13}$.

Sb1–O	2.086(4)	∠ O–Sb1–S2	94.11(12)
Sb1–S2	2.448(2)	∠ O–Sb1–S4	85.31(13)
Sb1–S4	2.4750(2)	∠ S2–Sb1–S4	100.59(6)
Sb2–S1	2.7958(5)	∠ S5–Sb2–S1	86.56(4)
Sb2–S5	2.428(2)	∠ S5–Sb2–S6	89.07(5)
Sb2–S6	2.769(2)	∠ S6–Sb2–S1	175.31(4)
Sb2–S7	2.393(2)	∠ S7–Sb2–S1	88.23(4)
Sb3–O	2.022(4)	∠ S7–Sb2–S5	97.78(6)
Sb3–S3	2.393(2)	∠ S7–Sb2–S3	90.69(6)
Sb3–S4	2.858(2)	∠ O–Sb3–S3	98.65(13)
Sb2–S6	2.837(2)	∠ O–Sb3–S4	76.87(13)
		∠ O–Sb3–S6	77.08(13)
		∠ S3–Sb3–S4	96.39(5)
		∠ S3–Sb3–S6	88.89(6)
		∠ S4–Sb3–S6	153.92(5)

Table S2. Structural features of Sb-based oxychalcogenides.

Compounds	Space group	crystal system	Q-to-O ratio	BBUs	Structural dimension	Ref.
$La_6Sb_4O_{12}S_3$	*I* 4_1/*amd* (141)	orthorhombic	0.25	[SbO_3]	0D	13
$Ba_6Sb_6O_2S_{13}$	*P* 2_1/*c* (14)	monoclinic	6.5	[$SbOS_2$], [$SbOS_3$], [SbS_4]	0D	This work
$Ba_2Sb_2O_2S_3$	*C*2/*c* (15）		1.5	[$SbOS_2$]	0D	14
$Ca_2Sb_2O_2S_3$			1.5	[$SbOS_4$]	1D	14
$Sr_2Sb_2O_2Se_3$			1.5	[$SbOSe_4$]	1D	15
$Sr_6Cd_2Sb_6O_7Se_{10}$	*Cm* (8)		1.43	[SbO_4], [$SbOSe_4$], [$SbSe_5$]	1D+2D	16
$Sr_6Cd_2Sb_6O_7S_{10}$			1.43	[SbO_4], [$SbOS_4$], [SbS_5]	1D+2D	17
$Pb_{13.43}Sb_{15.57}O_{0.18}S_{36}$	*C*2/*m* (12)		200	[SbS_5], [SbS_3], [$SbOS_3$], [SbO_3S]	2D	18
$Pb_{14}Sb_{30}O_5S_{54}$			10.8	[SbS_5], [SbS_3], [SbO_2S_2]		19
$CeSbOS_2$	*P*2_1/*m* (11)		2	[SbS_3]		20
$SrCuSbOS_2$			2	[$SbOS_4$]		21
$SrCuSbOSe_2$			2	[$SbOSe_4$]		22
$Sr_{3.5}Pb_{2.5}Sb_6O_5S_{10}$			2	[SbO_2S_2]		23
$Sr_4Pb_{1.5}Sb_5O_5Se_8$	*Cm* (8)		1.6	[SbO_3]		24
$CaSb_{10}O_{10}S_6$	*C*2/*c* (15)		0.6	[SbO_3], [$SbOS_2$], [SbS_3], [SbO_4]	3D	25

4. References

(1) G. Kortüm, *Reflectance Spectroscopy*; Springer-Verlag: NewYork, 1969.

(2) K. A. Borup, J. D. Boor, H. Wang, F. Drymiotis, F. Gascoin, X. Shi, L. D. Chen, M. I. Fedorov, E. Müller, B. B. Iversen and G. J. Snyder, Measuring thermoelectric transport properties of materials. *Energy Environ. Sci.*, 2015, **8**, 423–435.

(3) *CrystalClear* Version 1.3.5; Rigaku Corp.: Woodlands, TX, 1999.

(4) Sheldrick, G. M. A short history of SHELX, *Acta Crystallogr., Sect. A: Found. Crystallogr.,* 2008, 112–122.

(5) A. L. Spek, Single-crystal structure validation with the program PLATON, *J. Appl. Cryst.,* 2003, **36**, 7–13.

(6) L. M. Gelato and E. *J.* Parthe, STRUCTURE TIDY–a computer program to standardize crystal structure data, *Appl. Crystallogr.,* 1987, **20**, 139–143.

(7) G. Kresse, VASP, 5.3.5; http://cms.mpi.univie.ac.at/vasp/vasp/vasp.html.

(8) G. Kresse and J. Furthmuller, Efficient iterative schemes for ab initio total-energy calculations using a plane-wave basis set, *Phys. Rev. B: Condens. Matter,* 1996, **54**, 11169–11186.

(9) G. Kresse and D. Joubert, From ultrasoft pseudopotentials to the projector augmented-wave method, *Phys. Rev. B: Condens. Matter,* 1999, **59**, 1758–1775.

(10) J. P. Perdew, K. Burke and M. Ernzerhof, Generalized gradient approximation made simple, *Phys. Rev. Lett.,* 1996, **77**, 3865–3868.

(11) P. E. Blochl, Projector augmented-wave method, *Phys. Rev. B: Condens. Matter,* 1994, **50**, 17953–17979.

(12) D. J. Chadi, Special points for Brillouin-zone integrations. *Phys. Rev. B: Condens. Matter,* 1976, **16**, 1746–1747.

(13) W. W. So, A. LaCour, V. O. Aliev and P. K. Dorhout, Synthesis and characterization of a new quaternary lanthanum oxythioantimonite: $La_6Sb_4O_{12}S_3$. *J. Alloys Compd*., 2004, **374**, 234–239.

(14) R. Wang, Y. Zhao, X. Zhang and F. Huang, Structural dimension modulation in a new oxysulfide system of $Ae_2Sb_2O_2S_3$ (Ae = Ca and Ba). *Inorg. Chem. Front.*, 2022, **9**, 3552–3558.

(15) J. R. Panella, J. Chamorro and T. M. McQueen, Synthesis and Structure of Three New Oxychalcogenides: $A_2O_2Bi_2Se_3$ (A = Sr, Ba) and $Sr_2O_2Sb_2Se_3$. *Chem. Mater.*, 2016, **28**, 890–895.

(16) R. Wang, F. Wang, X. Zhang, X. Feng, C. Zhao, K. Bu,. Z. Zhang, T. Zhai and F. Q. Huang, Improved Polarization in the $Sr_6Cd_2Sb_6O_7Se_{10}$ Oxyselenide through Design of Lateral Sublattices for Efficient Photoelectric Conversion. *Angew. Chem. Int. Ed.* 2022, **61**, e202206816.

(17) R. Wang, F. Liang, F. Wang, Y. Guo, X. Zhang, Y. Xiao, K. Bu, Z. Lin, J. Yao, T. Zhai and F. Q. Huang, $Sr_6Cd_2Sb_6O_7S_{10}$: Strong SHG Response Activated by Highly Polarizable Sb/O/S Groups. *Angew. Chem. Int. Ed., 2019,* **58**, 8078–8081.

(18) D. Topa, J. Sejkora, E. Makovicky, J. Prsek, D. Ozdin, H. Putz, H. Dittrich and S. Karup-Moller, $Pb_{15-2x}Sb_{14+2x}S_{36}O_x$ (x similar to 0.2), a new sulphosalt species from the Low Tatra Mountains, Western Carpathians, Slovakia. *Eur. J. Mineral*., 2012, **24**, 727–740.

(19) Y. Moelo, A. Meerschaut, P. Orlandi and P. Palvadeau, Lead-antimony sulfosalts from Tuscany (Italy): II - Crystal structure of scainiite, $Pb_{14}Sb_{30}S_{54}O_5$, an expanded monoclinic derivative of $Ba_{12}Bi_{24}S_{48}$ hexagonal sub-type (zinkenite group). *Eur. J. Mineral*., 2000, **12**, 835–846.

(20) M. Nagao, M. Tanaka, R. Matsumoto, H. Tanaka, S. Watauchi,Y. Takano and I. Tanaka, Growth and Structure of $Ce(O,F)SbS_2$ Single Crystals. *Cryst. Growth Des.,* 2016, **16**, 3037–3042.

(21) K. Bu, M. Luo, R. Wang, X. Zhang, J. He, D. Wang, W. Zhao and F. Q. Huang, Enhanced Photoelectric $SrOCuSbS_2$ of a [SrO]-Intercalated $CuSbS_2$ Structure. *Inorg. Chem*., 2019, **58**, 69–72.

(22) K. Bu, J. Huang, M. Luo, M. Guan, C. Zheng, J. Pan, X. Zhang, S. Wang, W. Zhao, X. Shi, L. Xu and F.Q. Huang, Observation of High Seebeck Coefficient and Low Thermal Conductivity in New [SrO]-intercalated $CuSbSe_2$ Compound. *Chem. Mater.*, 2018, **30**, 5539–5543.

(23) R. Wang, K. Bu, X. Zhang, Y. Gu, Y. Xiao, Z. Zhan and F. Q. Huang, A Novel Two-Dimensional Oxysulfide $Sr_{3.5}Pb_{2.5}Sb_6O_5S_{10}$: Synthesis, Crystal Structure, and Photoelectric Properties. *J. Mater. Chem. C*, 2020, **8**, 11018–11021.

(24) Y. Wang, M. Luo, P. Zhao, X. Che, Y. Cao and F. Q. Huang, $Sr_4Pb_{1.5}Sb_5O_5Se_8$: a new mid-infrared nonlinear optical material with a moderate SHG response. *CrystEngComm*, 2020, **22**, 3526–3530.

(25) I. Nakai, K. Koto, K. Nagashima and N. Morimoto, The crystal structure of sarabauite $CaSb_{10}O_{10}S_6$, a new oxide sulfide mineral. *Chem. Letter.,* 1977, 275–276.